

Supplementary Material

Thermo- and pH-dual responsive polymeric micelles with upper critical solution temperature behavior for photoacoustic imaging guided synergistic chemophothermal therapy against subcutaneous and metastatic breast tumors

Zhe Yang^{a,†}, Rui Cheng^{a,†}, Chenyang Zhao^a, Na Sun^a, Huiyan Luo^c, Ya Chen^c, Zerong Liu^a, Xian Li^a, Jie Liu^{b,*}, Zhongmin Tian^{a,*}

^a *The Key Laboratory of Biomedical Information Engineering of Ministry of Education, School of Life Science and Technology, Xi'an Jiaotong University, Xi'an 710049, China*

^b *Department of Biomedical Engineering, School of Engineering, Sun Yat-sen University, Guangzhou, Guangdong 510006, China*

^c *Department of Medical Oncology, Sun Yat-sen University Cancer Center; State Key Laboratory of Oncology in South China, Guangzhou 510060, China*

† These authors contribute equally to this work.

* Corresponding author

* **E-mail:** liujie56@mail.sysu.edu.cn;

zmtian@xjtu.edu.cn

* **Tel:** 0086-20-3933-2145

0086-29-82667331

Supplementary Material

Table S1. The molecular weight and the molar ratio of acrylamide/acrylonitrile/1-vinylimidazole in P(AAm-*co*-AN-*co*-VIm) and mPEG-*b*-P(AAm-*co*-AN-*co*-VIm) copolymer

Polymer	Mn (g/mol)	PDI	Molar ratio of AAm : AN : VIm
PAAV	11896	1.69	62.3:37.7:10.7
mPEG-PAAV	16861	1.59	63.4:36.6:10.2

Supplementary Material

Table S2. Additive therapeutic efficacies of chemotherapy and photothermal therapy, which are estimated using the equation of $E_{\text{additive}} = 100\% - (f_{\text{chemo}} \times f_{\text{photothermal}}) \times 100\%$ (f is the fraction of surviving cells after each treatment).

Concentration ($\mu\text{g/mL}$)		Additive therapeutic efficacy (%)	Therapeutic efficacy of mPEG-PAAV micelles/IR780+DOX (%)
DOX	IR780		
0.4	0.3	91.55	92.51
0.2	0.15	74.83	80.46
0.1	0.075	61.64	64.13
0.05	0.0375	46.53	48.40
0.025	0.0187	28.32	29.11
0.0125	0.0093	18.36	16.40

Figure S1

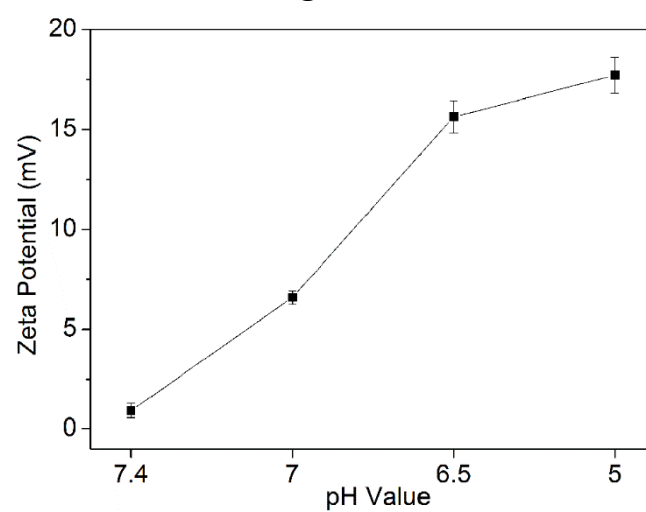


Figure S1. Zeta potential of mPEG-PAAV micelles at different pH values (n=3).

Figure S2

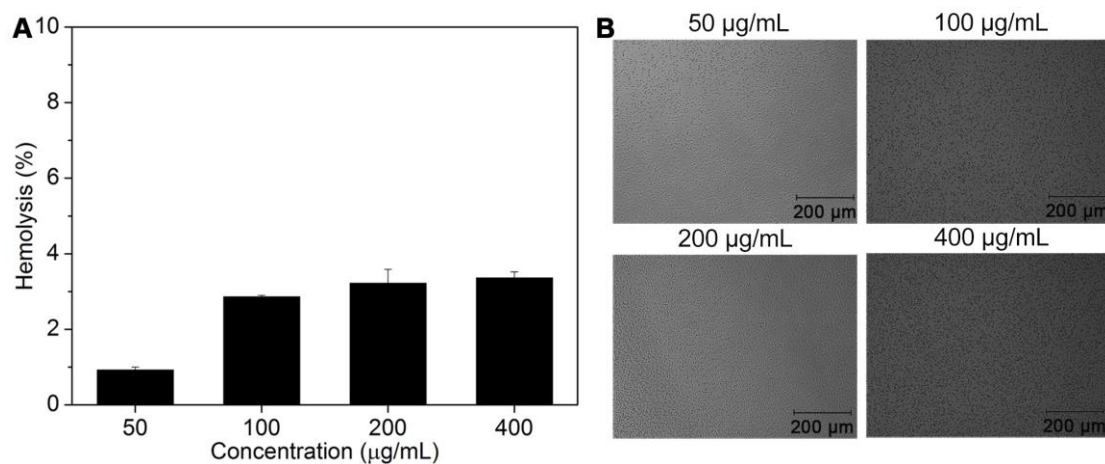


Figure S2. (A) Quantitative analysis on hemolytic activity and (B) microscopic images of the erythrocytes after the treatment of mPEG-PAAV micelles at different concentrations (n=3).

Figure S3

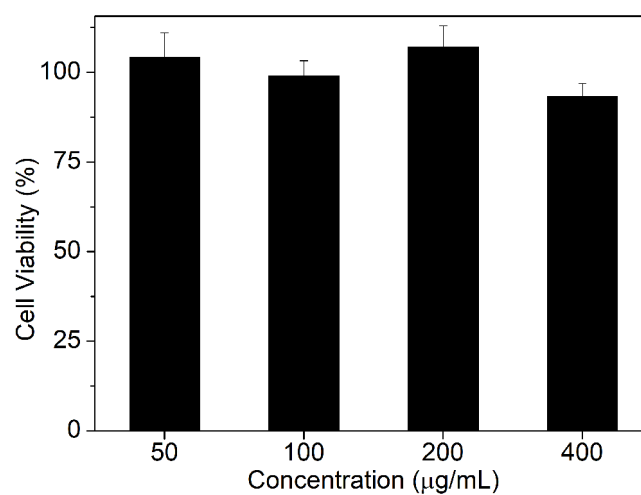


Figure S3. Viability of the 4T1 cells after the treatment of mPEG-PAAV micelles at different concentrations for 48 h (n=5).

Figure S4

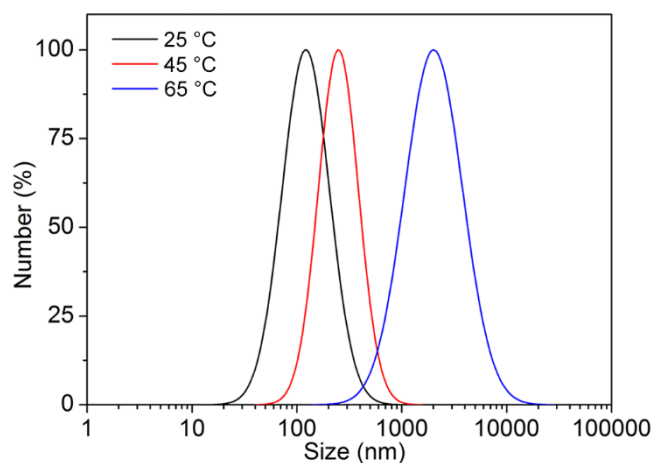


Figure S4. Size distribution of mPEG-PAAV micelles at different temperature (25 °C, 45 °C and 65 °C).

Figure S5

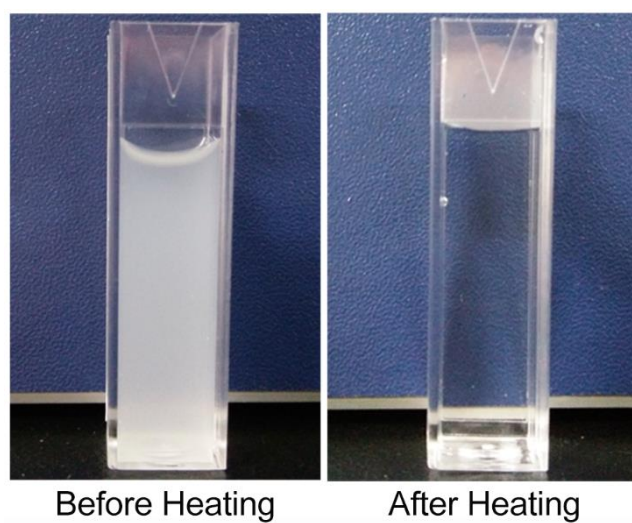


Figure S5. Turbidity of the mPEG-PAAV micelles solution before and after heating.

Figure S6

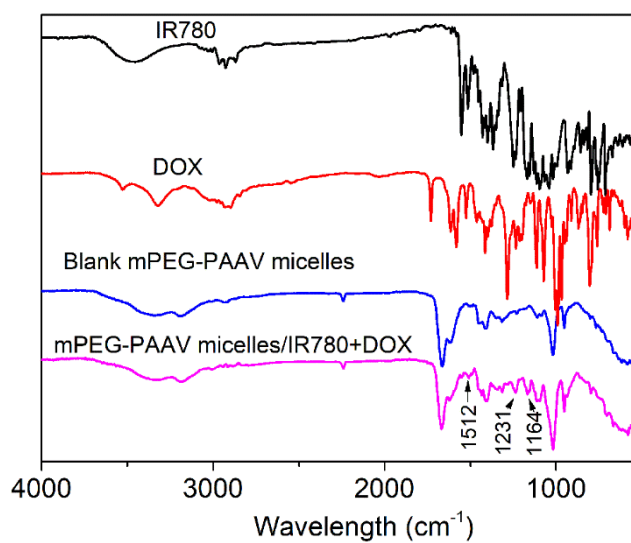


Figure S6. FTIR spectra of free DOX, free IR780, blank mPEG-PAAV micelles and mPEG-PAAV micelles/IR780+DOX.

Figure S7

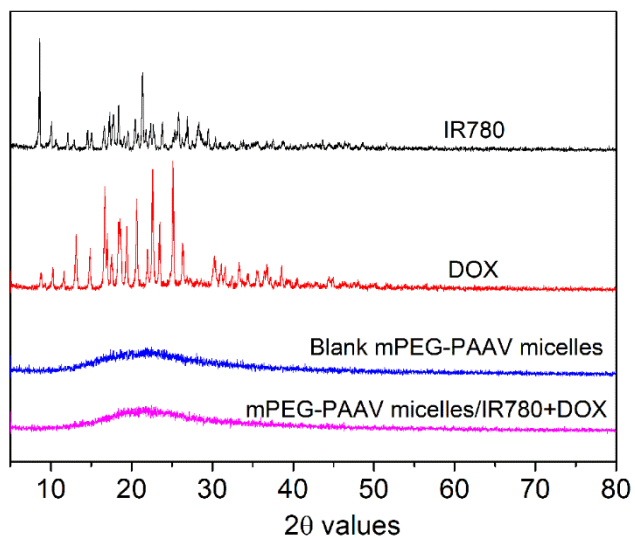


Figure S7. XRD spectra of free DOX, free IR780, blank mPEG-PAAV micelles and mPEG-PAAV micelles/IR780+DOX.

Figure S8

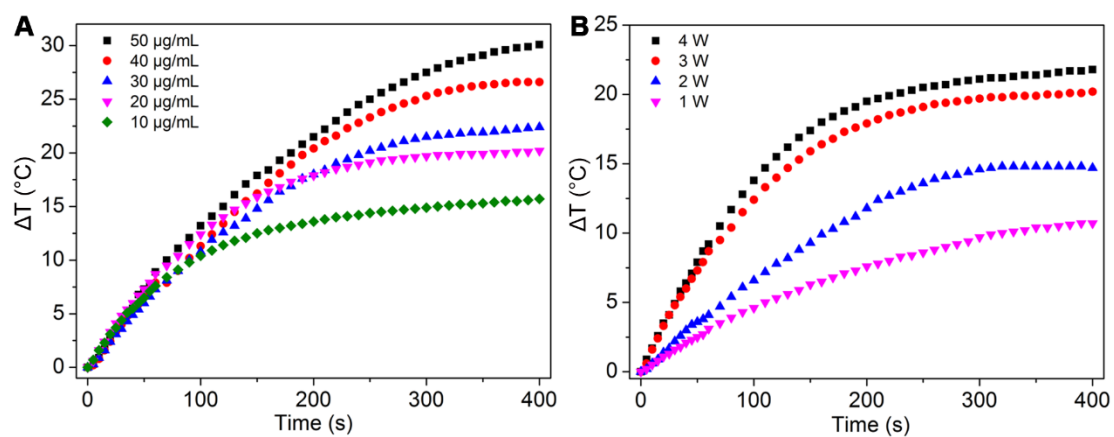


Figure S8. (A) Temperature changes of the mPEG-PAAV micelles at different concentrations under 808 nm laser irradiation (3 W/cm²); (B) temperature changes of the mPEG-PAAV micelles at 30 $\mu\text{g/mL}$ under 808 nm laser irradiation with different power.

Figure S9

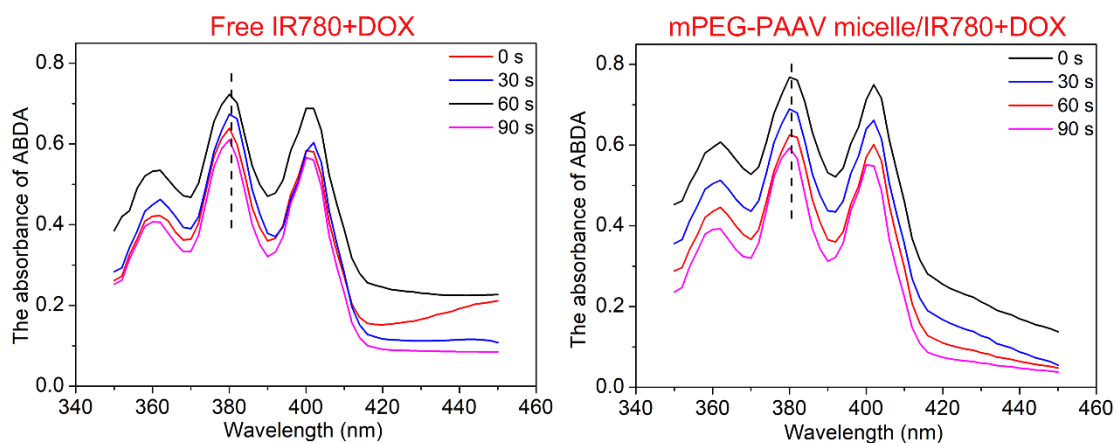


Figure S9. Absorbance of 9,10-anthracenediyl-bis(methylene) dimalonic acid (ABDA, 10^{-4} M) after photodecomposition by ROS generation upon 808 nm laser irradiation at 3 W/cm^2 in the presence of free IR780+DOX and mPEG-PAAV micelle/IR780+DOX at IR780 concentration of $10 \mu\text{g/mL}$. Briefly, due to ABDA could be oxidized in the presence of ROS, leading to the absorbance decrease of ABDA at 380 nm, ABDA solution (10^{-4} M) was added into the free IR780+DOX and mPEG-PAAV micelle/IR780+DOX solution and then irradiated with NIR laser (808 nm, 3 W/cm^2) for different times. Subsequently, the absorbance spectra of the above resultant solution were measured.

Figure S10

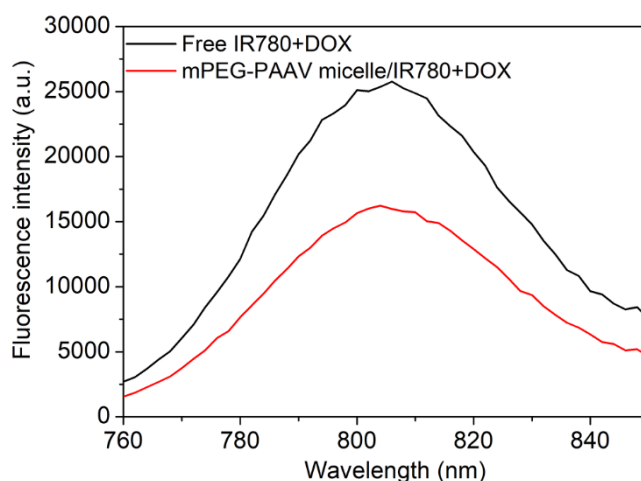


Figure S10. Fluorescence spectra (excitation wavelength at 740 nm) of free IR780+DOX and mPEG-PAAV micelle/IR780+DOX at IR780 concentration of 20 $\mu\text{g}/\text{mL}$. The fluorescence quenching efficiency of mPEG-PAAV micelle/IR780+DOX was calculated using the following equation: Fluorescence quenching efficiency = $(1 - (F_1 / F_2)) \times 100\%$, where F_1 and F_2 represent the fluorescence intensities of IR780 at 805 nm in mPEG-PAAV/IR780+DOX (F_1) and free IR780+DOX (F_2) groups, respectively.

Figure S11

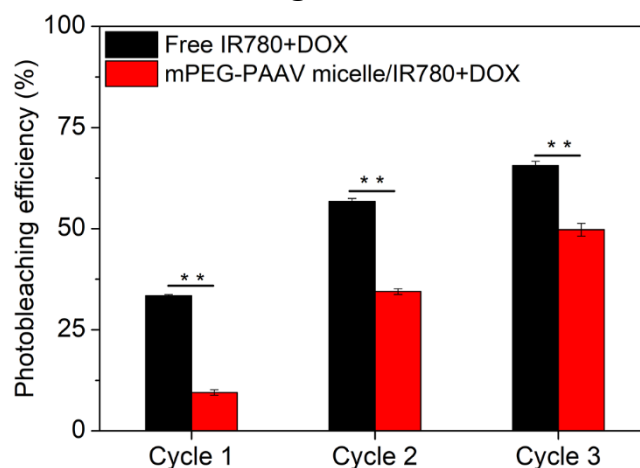


Figure S11. Photobleaching efficiency of free IR780+DOX and mPEG-PAAV/IR780+DOX after 3 cycles of NIR laser irradiation (808 nm, 3 W/cm², 1 min for each cycle) (n=3). Briefly, the fluorescence intensities of IR780 in free IR780+DOX and mPEG-PAAV/IR780+DOX groups at the same concentration of IR780 (20 µg/mL) were measured using fluorescence spectrometry (Hitachi F7000) at excitation wavelength of 740 nm and emission wavelength of 805 nm before and after NIR laser irradiation. And the photobleaching efficiency was calculated using the following equations: Photobleaching efficiency (%) = $F / F_0 \times 100\%$, where F_0 and F represent the fluorescence intensities of IR780 in free IR780+DOX or mPEG-PAAV/IR780+DOX group before and after NIR laser irradiation, respectively.

Figure S12

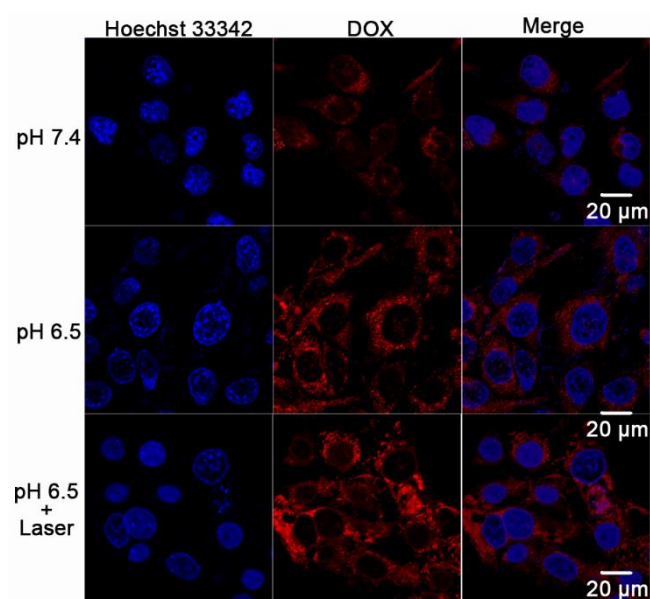


Figure S12. CLSM images of 4T1 cells treated with mPEG-PAAV micelles/IR780+DOX at pH 7.4 and 6.5 with or without 808 nm laser irradiation (3 W/cm², 5 min).

Figure S13

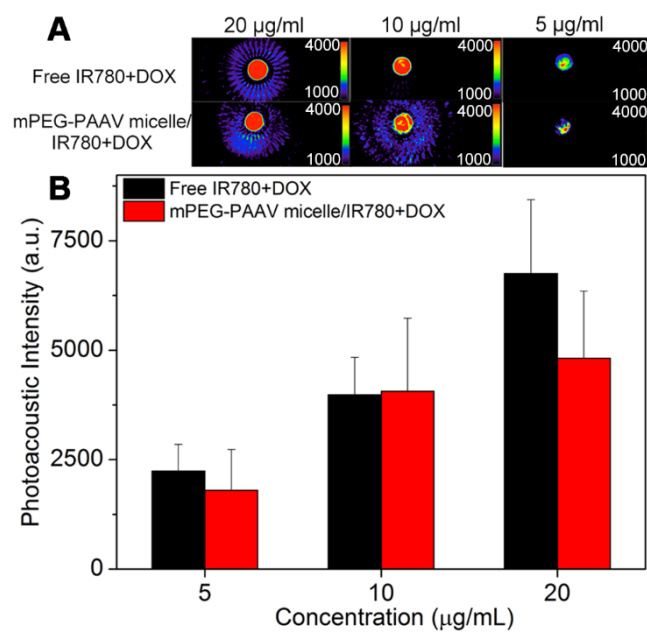


Figure S13. (A) and (B) PA images of free IR780+DOX and mPEG-PAAV micelles/IR780+DOX at different concentrations (n=3).

Figure S14

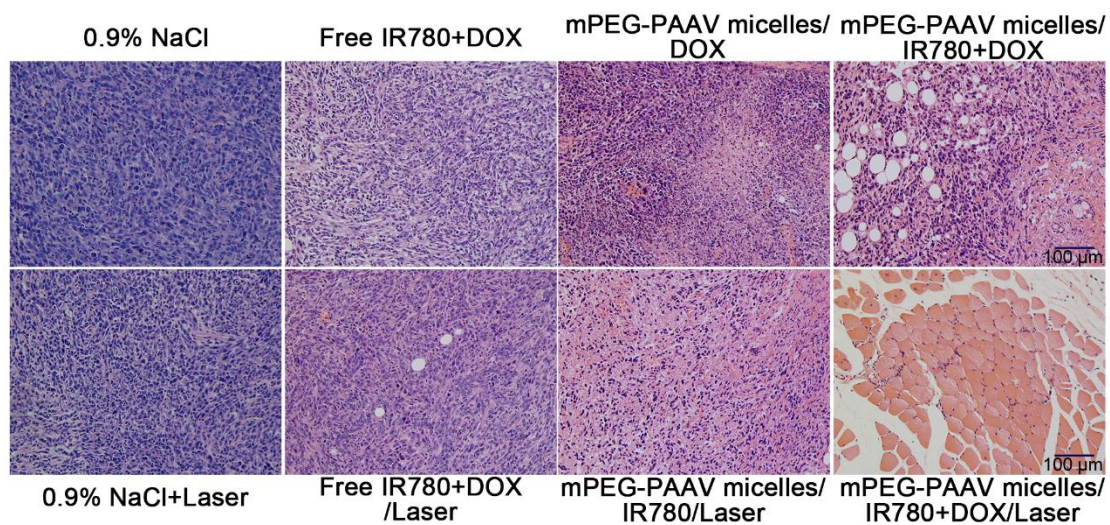


Figure S14. H&E staining analysis of tumor slices at the end of the treatment (29 day).

Figure S15

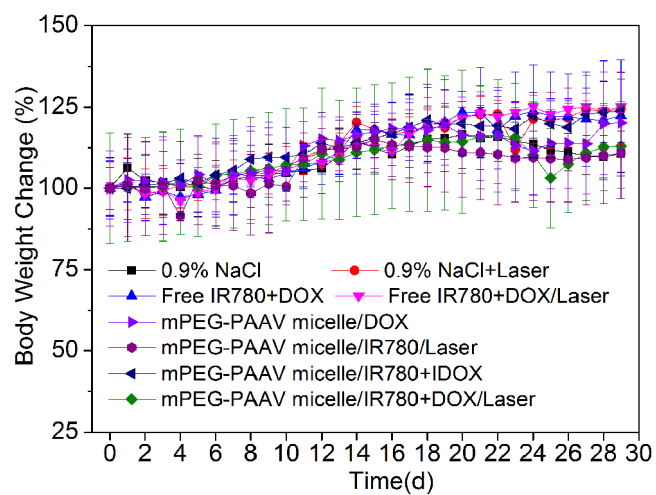


Figure S15. The changes in body weight during the experimental period (0~29 day) (n=5).

Figure S16

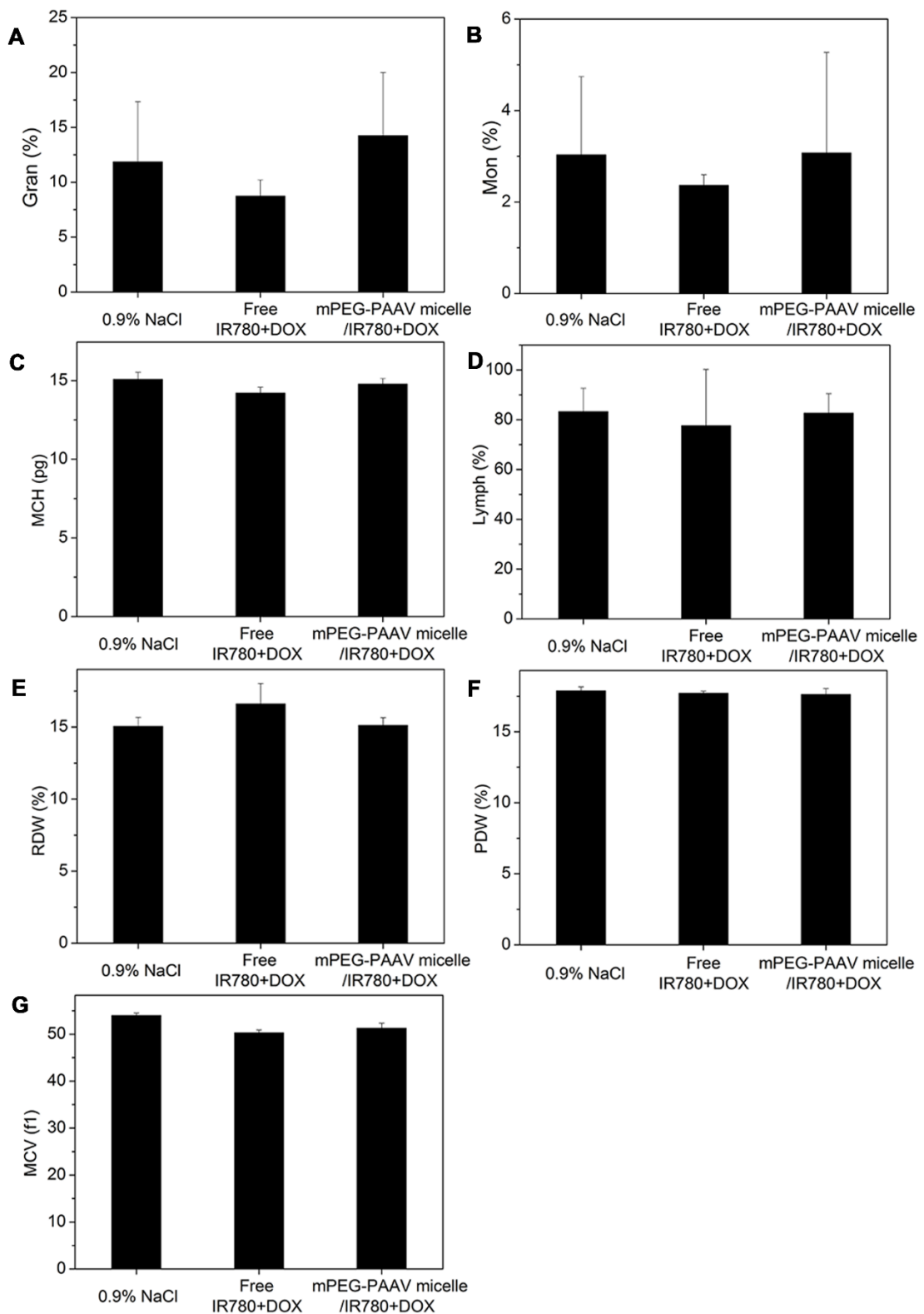


Figure S16. The routine blood examination on day 29 after the administration of 0.9% NaCl, free IR780+DOX and mPEG-PAAV micelles/IR780+DOX for three times (n=5).